

Time-dependent dynamical Bragg diffraction in crystals by beam propagation method (BPM)

Jacek Krzywinski and Aliaksei Halavanau

SLAC National Accelerator Laboratory, 2575 Sand Hill Road , Menlo Park CA 94025, USA

ABSTRACT

In this paper we describe how to solve time dependent x-ray dynamic diffraction problems in distorted crystal using a beam propagation method (BPM). We will show examples of using the BPM method to simulate propagation of x-ray beams in deformed crystals in space and time domain which are relevant to performance of x-ray optics at x-ray Free Electron Lasers

Keywords: x-ray dynamic diffraction, crystals, x-ray free electron lasers

1. INTRODUCTION

The Beam Propagation Method (BPM) is a popular method to simulate propagation and scattering of waves in a non-homogeneous media¹ and has been frequently used to simulate and design optoelectronic devices.²⁻⁷ The BPM methods can be roughly divided in two groups. The first group, called FD BPM, employs the finite difference method. The second group called FFT BPM uses fast Fourier transforms (FFT) to solve the governing equations. The FD BPM method is often used for problems where the wavelength is comparable with one of the dimensions of simulated elements or with a length of the pulse. The FFT BPM method is a method of choice when the slowly varying envelope approximation (SVEA) can be applied. The popularity of the BPM methods is attained by its relative simple algorithm and its straightforward way of modeling complicated optical elements by a spatial distribution of dielectric susceptibility. The other advantage of BPM is that it is formulated as an initial value problem and that the boundary conditions are automatically fulfilled.

The BPM method is well suited for modeling a large variety of problems dealing with highly coherent x-ray beams produced by x-ray free electron lasers (XFELs) or synchrotron radiation sources of 4th generation. A small value of x-ray susceptibility leads to simplifications of governing equations which could be even further simplified when para-axial approximation is justified. There is an increasing interest in applying BPM method for simulating propagation of highly coherent x-rays beams through complicated x-ray optics⁸⁻¹⁶

In this paper we will focus on FFT BPM which could be efficiently applied in time dependent simulations of XFEL pulses diffracted from deformed crystals of arbitrary shapes.

2. THEORETICAL APPROACH

The scalar Helmholtz equation for a constant angular frequency ω :

$$(\nabla^2 + k(n(x, y, z))^2) E(x, y, z) = 0 \quad (1)$$

can be written in the following form:^{1,5}

$$\frac{d\psi}{d\hat{z}} = i \left(\sqrt{1 + \nabla_{\perp}^2 - \delta\epsilon(\hat{x}, \hat{y}, \hat{z})} - 1 \right) \psi \quad (2)$$

where $\hat{x}, \hat{y}, \hat{z} = kx, ky, kz$, k is the wave vector, ∇_{\perp}^2 is the Laplace operator taken with respect to the transverse coordinates \hat{x}, \hat{y} , $\delta\epsilon(\hat{x}, \hat{y}, \hat{z}) = n(\hat{x}, \hat{y}, \hat{z})^2 - \bar{n}^2$, $n(\hat{x}, \hat{y}, \hat{z})$ is the refractive index, \bar{n} is its average value and

Further author information: (Send correspondence to J.K)
J.K: E-mail: krzywins@slac.stanford.edu

$E(x, y, z) = \psi(x, y, z)e^{-ikz}$. In the case of beams with narrow angular spectrum this equation can be approximated by:

$$\frac{d\psi}{d\hat{z}} = i \left(\sqrt{1 + \nabla_{\perp}^2} - \frac{\delta\epsilon(\hat{x}, \hat{y}, \hat{z})}{2\sqrt{1 - \langle k_x^2 + k_y^2 \rangle}} - 1 \right) \psi \quad (3)$$

Here the operator $\sqrt{1 + \nabla_{\perp}^2}$ in the denominator of the second term of the r.h.s was approximated by $\sqrt{1 - \langle k_x^2 + k_y^2 \rangle}$ where $\langle k_x^2 + k_y^2 \rangle$ is the average angular spectrum and $k_x^2 + k_y^2 = F[\nabla_{\perp}^2]$ is the Fourier transform of the ∇_{\perp}^2 operator. Equation (3) leads to the following FFT BPM propagation equation:

$$\psi(\hat{x}, \hat{y}, \hat{z} + \Delta\hat{z}) \approx F^{-1} \left\{ F[\psi(\hat{x}, \hat{y}, \hat{z})] e^{i\Delta\hat{z}\sqrt{1 - k_x^2 - k_y^2}} \right\} e^{i\Delta\hat{z}\frac{\delta\epsilon(\hat{x}, \hat{y}, \hat{z})}{2} / \cos\alpha} \quad (4)$$

where F and F^{-1} denote Fourier and inverse Fourier transforms, $\cos\alpha = \sqrt{1 - \langle k_x^2 + k_y^2 \rangle}$. The angle α corresponds to the grazing incidence angle with respect to the propagation direction. We have previously applied Eq. (4) to take into account dynamic diffraction effects when simulating interaction of x-ray beams with gratings and multilayer optics.⁸⁻¹¹

2.1 Application to crystal diffraction

In large class of dynamical diffraction problems the angular spectrum of the scattered x-ray beams consists of two narrow bands centred around the incident and the reflection angles. The meaningful information is contained within these bands. This allows to remove the fast oscillating component, related to inter-planar spacing, from the physical picture and derive FFT BPM equations for slowly varying envelopes of transmitted and reflected beams. For simplicity we are considering the 2D (x,z) case. The generalization for the 3D case is straightforward. The procedure is outlined below. First, one can write the the scattered x-ray field as a sum of of two components:

$$\psi(\hat{z}, \hat{x}) = \psi(\hat{z}, \hat{x})_+ + \psi(\hat{z}, \hat{x})_- \quad (5)$$

Then the slowly varying envelopes are defined as follows:

$$\tilde{\psi}(\hat{z}, \hat{x})_+ = \psi(\hat{z}, \hat{x})_+ e^{-i\frac{k_d}{2}\hat{x}}, \quad \tilde{\psi}(\hat{z}, \hat{x})_- = \psi(\hat{z}, \hat{x})_- e^{i\frac{k_d}{2}\hat{x}} \quad (6)$$

where k_d is the reciprocal vector related to inter-planar spacing. Next we expand the exponential term related to dielectric susceptibility in Eq. (4) as:

$$e^{i\hat{z}\frac{\delta\epsilon(\hat{z}, \hat{x})}{2\cos\alpha}} = \sum_n \Delta\epsilon(\hat{z}, \hat{x})_n e^{ik_d n \hat{x}} \quad (7)$$

For the symmetric Bragg case the first three terms of this expansion can be written in the form:

$$\Delta\epsilon_0 = J_0 \left(2z \frac{(|\chi_{rh}| - i|\chi_{ih}|)}{2\cos\alpha} \Pi(x, z) \right) e^{\frac{iz}{2\cos\alpha} \chi_0 \Pi(x, z)} \quad (8)$$

$$\Delta\epsilon_1 = \Delta\epsilon_{-1} = iJ_1 \left(2z \frac{(|\chi_{rh}| - i|\chi_{ih}|)}{2\cos\alpha} \Pi(x, z) \right) e^{\frac{iz}{2\cos\alpha} \chi_0 \Pi(x, z)} \quad (9)$$

where $\Pi(x, z) = 1$ inside the crystal and $\Pi(x, z) = 0$ outside the crystal. χ_0 , χ_{rh} and χ_{ih} are complex polarizabilities of an ideal absorbing crystals determined for a given reflection.

Here we applied Jacobi–Anger expansion:

$$e^{iz\cos\theta} = \sum_{n=-\infty}^{\infty} i^n J_n(z) e^{in\theta} \quad (10)$$

For the Bragg reflection case we can describe the $\delta\epsilon(\hat{z}, \hat{x})$ in Eq. (11) as a complex harmonic function with the period equal to the inter-planar spacing:

$$\delta\epsilon(\hat{z}, \hat{x}) = \chi_0 + 2\chi_h \cos k_d \hat{x} \quad (11)$$

and $\chi_0 = \chi_{0r} + i\chi_{0h}$ and $\chi_h = |\chi_{rh}| - i|\chi_{ih}|$. The complex amplitude is composed from the χ_{0r} , χ_{0h} , χ_{rh} and χ_{ih} which could be found for example at the web page “x-ray dynamical diffraction data on the web” (<https://x-server.gmca.aps.anl.gov/x0h.html>) or XOP x-ray optics software toolkit.¹⁷ We treat deformation of the crystal as modification of the susceptibility:¹⁸

$$\Delta\epsilon'_n(\hat{z}, \hat{x}) = \Delta\epsilon_n(\hat{z}, \hat{x})e^{i\mathbf{k}_d\mathbf{u}(\hat{z}, \hat{x})} \quad (12)$$

where $\mathbf{k}_d\mathbf{u}$ is a scalar product of the reciprocal and displacement vectors. Inserting Eq. (12) into Eq. (4) and neglecting terms proportional to $e^{ik_d n \hat{x}}$ for $|n| > 1$ one arrives at the following set of equations for slowly varying envelopes $\tilde{\psi}(\hat{z}, \hat{x})_+$ and $\tilde{\psi}(\hat{z}, \hat{x})_-$:

$$\begin{aligned} \tilde{\psi}(\hat{z} + \Delta\hat{z}, \hat{x})_+ &= \tilde{\psi}(\hat{z}, \hat{x})_{p+} \Delta\epsilon_0(\hat{z}, \hat{x}) + \tilde{\psi}(\hat{z}, \hat{x})_{p-} \Delta\epsilon'_{+1}(\hat{z}, \hat{x}) \\ \tilde{\psi}(\hat{z} + \Delta\hat{z}, \hat{x})_- &= \tilde{\psi}(\hat{z}, \hat{x})_{p-} \Delta\epsilon_0(\hat{z}, \hat{x}) + \tilde{\psi}(\hat{z}, \hat{x})_{p+} \Delta\epsilon'_{-1}(\hat{z}, \hat{x}), \end{aligned} \quad (13)$$

where $\tilde{\psi}(\hat{z}, \hat{x})_{p\pm} = F^{-1} \left[F \left[\tilde{\psi}(\hat{z}, \hat{x})_{\pm} \right] p_{\mp} \right]$. The operators $p_{\pm} = e^{i\Delta\hat{z} \sqrt{1 - (k_x \pm \frac{k_d}{2})^2}}$ correspond to the Fourier image of ∇_{\perp}^2 which is shifted by $\pm \frac{k_d}{2}$ in the angular spectrum space. Equation (4) can be rewritten in the operator form as:

$$\begin{aligned} \psi(\hat{x}, \hat{y}, \hat{z} + \Delta\hat{z}) &\approx \prod_i A(a_i \Delta z) B(b_i \Delta z) \psi(\hat{x}, \hat{y}, \hat{z}), \\ A &= F^{-1} \left\{ F [\psi(\hat{x}, \hat{y}, \hat{z})] e^{i a_i \Delta \hat{z} \sqrt{1 - k_x^2 - k_y^2}} \right\}, \\ B &= e^{i b_i \Delta \hat{z} \frac{\delta\epsilon(\hat{x}, \hat{y}, \hat{z})}{2} / \cos \alpha}. \end{aligned} \quad (14)$$

In case when $a_1 = 1, b_1 = 1$, or first order splitting, Eq. (14) is reduced to Eq. (4). For the most of the practical problems this splitting scheme is accurate. Higher order splittings are often needed for large Bragg angles, or backscattering. For instance, when $a_1 = 0.0, a_2 = 1.0, b_1 = 0.5, b_2 = 0.5$ Eq. (14) is accurate up to $O(\Delta z^2)$, and when $t = 1.3512, a_1 = 0.0, a_2 = t, a_3 = 1 - 2t, a_4 = t, b_1 = t/2, b_2 = (1 - t)/2, b_3 = (1 - t)/2, b_4 = t/2$ it is accurate up to $O(\Delta z^4)$. Finally, to further improve the accuracy in the split-operator scheme, we introduced a Zassenhaus-like exponent¹⁹ in Eq. (7):

$$\Delta\epsilon'_0 = \Delta\epsilon_0 e^{\frac{D_2}{2} \Delta z^2}, \quad D_2 = (\chi_h / 2.0 / \cos \alpha)^2 \quad (15)$$

This exponent allows for much larger Δz steps and faster computation while maintaining numerical accuracy.

We point out that Eqs. (13) can be treated as two beam approximation for the FFT BPM. These equations are analogous to the Takagi-Taupin equations (TTE) in two beam approximation.¹⁸ However, there is a significant difference between TTE and FFT BPM equations. The TTE equations are a system of hyperbolic equations where the second derivatives in the transverse direction with respect to the beam propagation are neglected. Therefore diffraction of the x-rays is not taken into account in the TTE formulation. The numerical algorithms for solving TTE, that are presented in the literature, typically require settings the boundary conditions which could be a difficult problem itself in complicated geometries or when the boundaries are not very well defined. On the other hand the FFT BPM equations is a system of parabolic equations that automatically includes diffraction. Also, as we have mentioned before the FFT BPM method is especially convenient when dealing with complicated shapes or non-homogeneous boundaries.

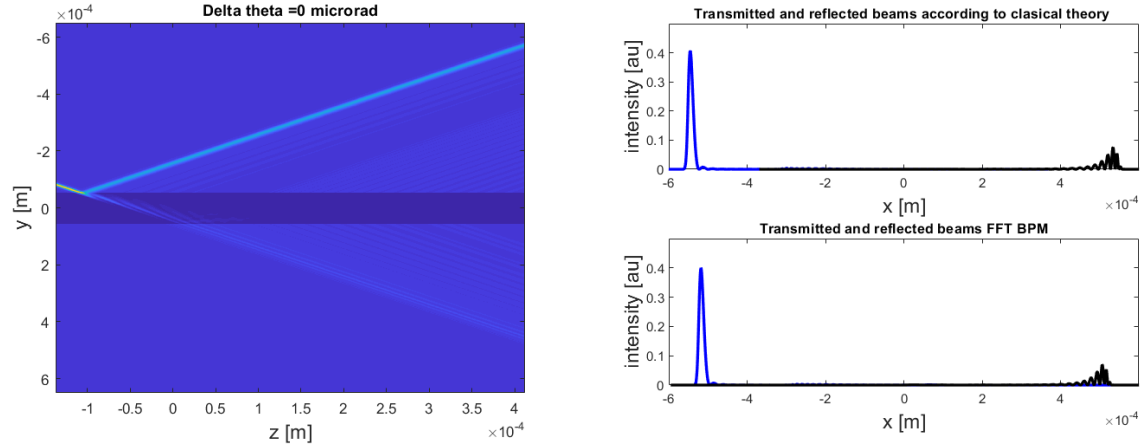


Figure 1. Left: 2D visualizations of a Bragg reflection. The incident has the transverse rms size of $3.5 \mu\text{m}$ which is smaller than the extinction length. Right: comparison of transverse profiles of transmitted and reflected beams obtained from FFT BPM and classical diffraction theory.²⁰

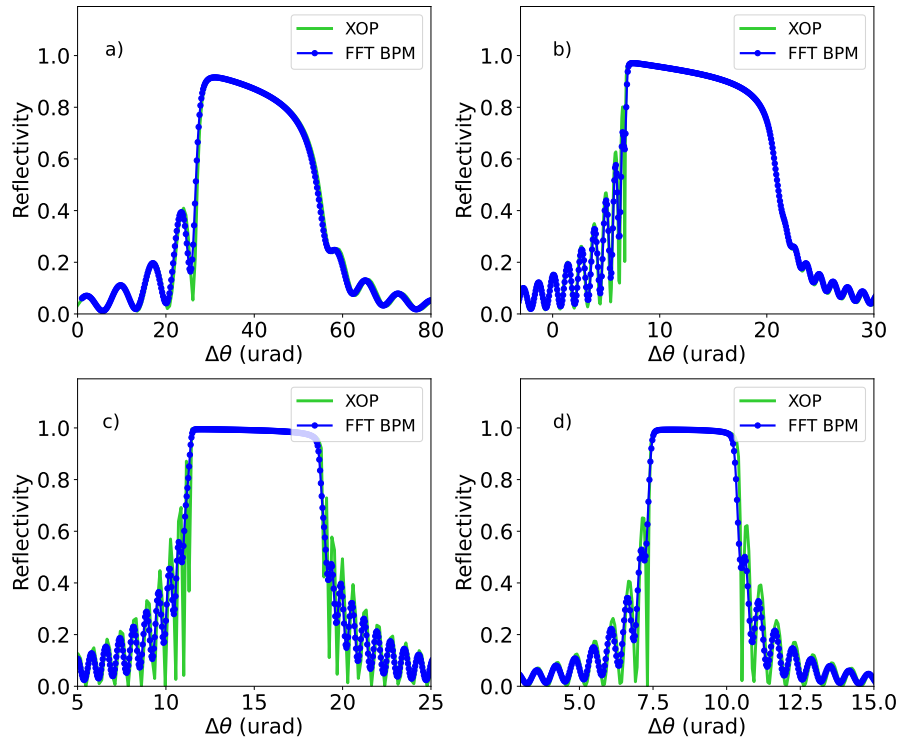


Figure 2. a) Si (444) reflection at 8048 eV, $\theta_B = 79^\circ$ b) Si (400) reflection at 9000 eV, $\theta_B = 30.5^\circ$ c) $C^*(400)$ reflection at 9853 eV, $\theta_B = 45^\circ$ d) $C^*(333)$ reflection at 12800 eV, $\theta_B = 44.9^\circ$.

3. NUMERICAL EXAMPLES

3.1 Stationary problems

We applied our implementation of FFT BPM based on Eqs.(8) to simulate $C^*(004)$ reflection and transmission of an x-ray beam scattered from a $100 \mu\text{m}$ thick crystal. We have chosen the transverse size of the Gaussian x-ray beam to be smaller than the extinction length in order to observe both the reflected, and the transmitted beam. We have compared results of our FFT BPM simulation with the the results based on the classical dynamic diffraction theory²⁰ and found a very good agreement. This can be seen in Fig.1 We have also checked the

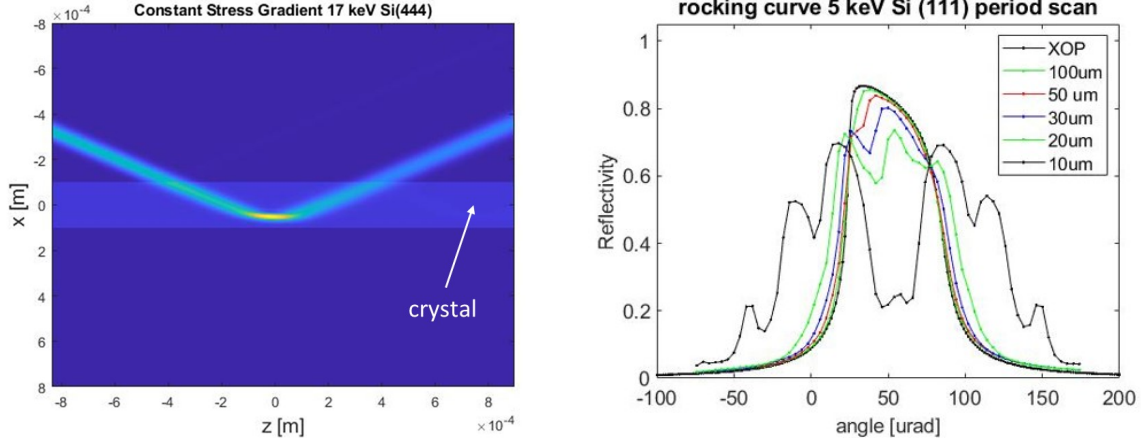


Figure 3. Left: 2D visualization of a Si(444) Bragg reflection with a constant strain gradient in the crystal. Right: Rocking curves simulated for a crystal with sinusoidal deformation having a constant amplitude of 1 Angstrom and different periods.

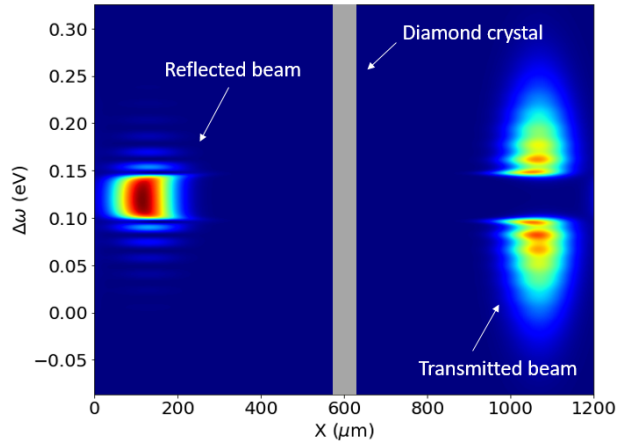


Figure 4. Diamond $C^*(333)$ reflected and transmitted beam for the case of incident Gaussian beam with $\sigma_t = 10$ fs, $W_0 = 50 \mu\text{m}$, $\omega_0 = 12800$ eV, and $50 \mu\text{m}$ thick crystal.

accuracy of our method by comparing rocking curves obtained by the FFT BPM method and the XOP software toolkit results. For this test, we consider a planar radiation intensity distribution:

$$\psi_{xy}^i(x, y) = \frac{1}{(1 + iz_x/z_R)} e^{-\frac{(x-x_0)^2 + y^2}{W_0^2(1+iz_x/z_R)}} e^{ix \sin \theta_i} \quad (16)$$

incident on a crystal, where z_x is distance to the source point, z_R is the Rayleigh range, W_0 is the Gaussian waist size and θ_i is the incidence angle. Example results simulated for Silicon and Diamond crystals are illustrated in Fig. 2. We point out a good agreement with XOP, e.g. even in the case of backscattering with the Bragg angle $\theta_B = 79^\circ$ shown in Fig. 2 a) FFT BPM corroborates with XOP results. The slight remaining discrepancies between FFT BPM and XOP are attributed to the fact that in our simulations we use finite Gaussian beams with angular divergence while XOP employs plane waves. The latter fact illustrates another advantage of FFT BPM in cavity-based systems with thin crystals, where the accuracy of modelling the spectral/temporal field profile is crucial.

In case of deformed crystals the deformation can be easily described by the distribution of $\Delta\epsilon'_n(\hat{z}, \hat{x})$, $n=1,0,1$. An example of constant strain gradient reflection is shown in Fig. 3 (left). Another example is presented

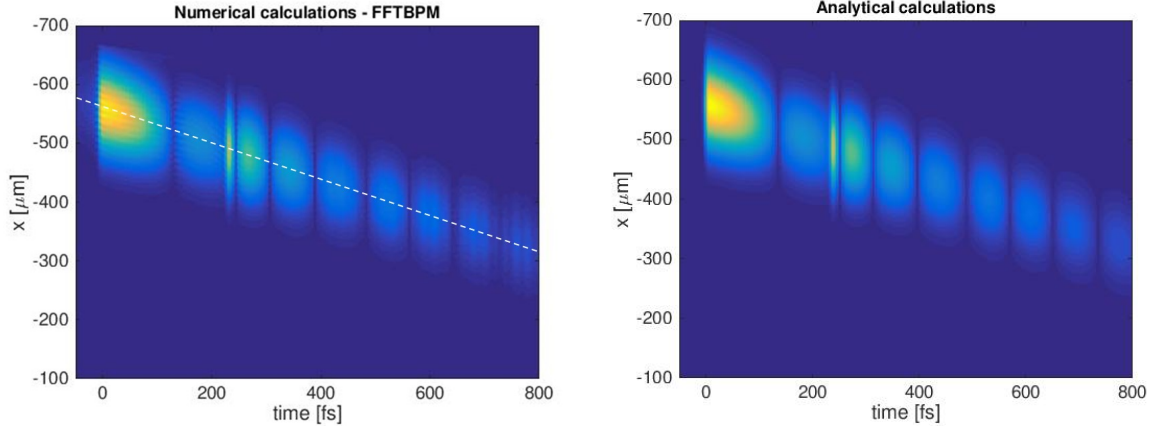


Figure 5. Spatio-temporal intensity profiles of the Bragg diffracted beam. Left: simulated with the FFT BPM method. Right: simulated using theory presented in.²⁰ The dashed line has a slope $-c \cot \theta_B$ predicted theoretically in.²⁰

in Fig 3 (right). Here the deformation of the crystal has a form of sinusoidal undulations of the amplitude of 1 Angstrom. We have simulated the rocking curves as a function of undulation period for the Si(111) reflection at 5 keV photon energy. The sample was illuminated by a Gaussian beam having a waist of $W_0=85.4 \mu\text{m}$ and located $z_x = 181.1 \text{ m}$ away from the sample.

3.2 Time-dependent problems

We now consider an incident time-dependent radiation field:

$$\psi_{txy}^i(t, x, y) = \frac{1}{\sqrt{2\pi}\sigma_t} \psi_{xy}^i e^{(t-t_0)^2/2\sigma_t^2}. \quad (17)$$

The field in Eq. (17) is Fourier transformed as $\psi_{\omega xy}^i(\omega, x, y) = \sum_{i=0}^N \psi_{t_i xy}^i(t_i, x, y) e^{i\omega t_i} \Delta t$, where N is the number of grid points, thereby transforming a time-dependent diffraction problem into N stationary problems with a given ω_i and the spatial intensity distribution ψ_{xy} . After the simulation, the diffracted field is obtained via an inverse Fourier transform $\psi_{txy}^h(t, x, y) = \sum_{i=0}^N \psi_{\omega_i xy}^h(\omega_i, x, y) e^{-i\omega_i t} \Delta\omega$. Figs. 4, 5 illustrate spatio-spectral and spatio-temporal responses of the $50 \mu\text{m}$ thick $C^*(333)$ crystal reflection to the incident Gaussian beam of $\omega_0 = 12800 \text{ eV}$. The detailed time-dependent analysis of Bragg diffraction in deformed crystals will be published elsewhere.

4. ACKNOWLEDGEMENTS

This work is supported by the U.S. Department of Energy Office of Science under Contract No. DE-AC02-76SF00515. This research used resources of the National Energy Research Scientific Computing Center (NERSC), a U.S. Department of Energy Office of Science User Facility located at Lawrence Berkeley National Laboratory, operated under Contract No. DE-AC02-05CH11231 using NERSC award ERCAP0020725.

REFERENCES

- [1] Ersoy, O. K., [*Diffraction, Fourier Optics and Imaging*], John Wiley I& Sons, Ltd (2007).
- [2] Sziklas, E. A. and Siegman, A. E., “Mode calculations in unstable resonators with flowing saturable gain. 2: Fast fourier transform method,” *Appl. Opt.* **14**, 1874–1889 (Aug 1975).
- [3] Feit, M. D. and Fleck, J. A., “Light propagation in graded-index optical fibers,” *Appl. Opt.* **17**(24), 3990–3998 (1978).
- [4] Shaaban, A., Sayed, M., Hameed, M. F. O., Saleh, H. I., Gomaa, L., Du, Y.-C., and Obayya, S., “Fast parallel beam propagation method based on multi-core and many-core architectures,” *Optik* **180**, 484 – 491 (2019).
- [5] Hadley, G. R., “Wide-angle beam propagation using padé approximant operators,” *Opt. Lett.* **17**(20), 1426–1428 (1992).
- [6] Yamauchi, J., Shibayama, J., and Nakano, H., “Fast-fourier transform beam-propagation method using fadé approximant operators,” *Electronics and Communications in Japan (Part II: Electronics)* **78**(3), 12–18 (1995).
- [7] Scalora, M. and Crenshaw, M. E., “A beam propagation method that handles reflections,” *Optics Communications* **108**(4), 191 – 196 (1994).
- [8] Gaudin, J., Ozkan, C., Chalupský, J., Bajt, S., Burian, T., Vyšín, L., Coppola, N., Farahani, S. D., Chapman, H. N., Galasso, G., Hájková, V., Harmand, M., Juha, L., Jurek, M., Loch, R. A., Möller, S., Nagasono, M., Störmer, M., Sinn, H., Saksl, K., Sobierajski, R., Schulz, J., Sovak, P., Toleikis, S., Tiedtke, K., Tschentscher, T., and Krzywinski, J., “Investigating the interaction of x-ray free electron laser radiation with grating structure,” *Opt. Lett.* **37**(15), 3033–3035 (2012).
- [9] Andrejczuk, A., Krzywinski, J., and Bajt, S., “Influence of imperfections in a wedged multilayer laue lens for the focusing of x-rays investigated by beam propagation method,” *Nuclear Instruments and Methods in Physics Research Section B: Beam Interactions with Materials and Atoms* **364**, 60 – 64 (2015).
- [10] Morgan, A. J., Prasciolu, M., Andrejczuk, A., Krzywinski, J., Meents, A., Pennicard, D., Graafsma, H., Barty, A., Bean, R. J., Barthelmess, M., Oberthuer, D., Yefanov, O., Aquila, A., Chapman, H. N., and Bajt, S., “High numerical aperture multilayer laue lenses,” *Scientific Reports* **5**(1), 9892 (2015).
- [11] Bajt, S., Prasciolu, M., Morgan, A. J., Chapman, H. N., Krzywinski, J., and Andrejczuk, A., “One dimensional focusing with high numerical aperture multilayer laue lens,” *AIP Conference Proceedings* **1696**(1), 020049 (2016).
- [12] Li, K., Wojcik, M., and Jacobsen, C., “Multislice does it all - calculating the performance of nanofocusing x-ray optics,” *Opt. Express* **25**(3), 1831–1846 (2017).
- [13] Yan, H., Kang, H. C., Conley, R., Liu, C., Macrander, A., Stephenson, G., and Maser, J., “Multilayer laue lens: A path toward one nanometer x-ray focusing,” *X-Ray Optics and Instrumentation* **2010** (2010).
- [14] Pfeiffer, F., David, C., van der Veen, J. F., and Bergemann, C., “Nanometer focusing properties of fresnel zone plates described by dynamical diffraction theory,” *Phys. Rev. B* **73**, 245331 (2006).
- [15] Marcus et.al., G., “Refractive guide switching a regenerative amplifier free-electron laser for high peak and average power hard x rays,” *Phys. Rev. Lett.* **125**, 254801 (Dec 2020).
- [16] Halavanau et.al., A., “Population inversion x-ray laser oscillator,” *Proceedings of the National Academy of Sciences* **117**(27), 15511–15516 (2020).
- [17] del Rio, M. S. and Dejus, R. J., “Xop v2.4: recent developments of the x-ray optics software toolkit,” *Proc.SPIE* **8141**, 8141 – 8141 – 5 (2011).
- [18] Authier, A., [*Dynamical Theory of X-Ray Diffraction*], International Union of Crystallography Monographs on Crystallography, Oxford University Press, Oxford (2003).
- [19] Casas, F., Murua, A., and Nadinic, M., “Efficient computation of the zassenhaus formula,” *Computer Physics Communications* **183**(11), 2386–2391 (2012).
- [20] Shvyd’ko, Y. and Lindberg, R., “Spatiotemporal response of crystals in x-ray bragg diffraction,” *Phys. Rev. ST Accel. Beams* **15**, 100702 (2012).